Nanoscale Research Letters

NANO EXPRESS Open Access

# Synthesis, Characterization, and Evaluation of Redox-Sensitive Chitosan Oligosaccharide Nanoparticles Coated with Phycocyanin for Drug Delivery

Ziting Cheng[1†], Wei Zhang[2†], Xiaoya Hou[1], Bingjie Wang[1], Yanping Zhu[1], Peng Zhang[1], Feng Zhao[1] and Daquan Chen[1*]

## Abstract

In this paper, a type of phycocyanin (PC)-functionalized and curcumin (CUR)-loaded biotin-chitosan oligosaccharide-dithiodipropionic acid-curcumin (BCSC) nanoparticles, called CUR-BCSC@PCs, were designed to enhance the biocompatibility of CUR. The structure of BCSC was confirmed using $^{1}$H-NMR. In CUR-BCSC@PCs with an average hydrodynamic diameter of 160.3 ± 9.0 nm, the biomimetic protein corona gave the nanoparticles excellent stability and the potential to avoid protein adsorption in blood circulation. The in vitro release experiment verified that CUR-BCSC@PCs with redox responsive shells were sensitive to high concentrations of glutathione. In addition, CUR-BCSC@PCs were effective at increasing the inhibitory activity on the proliferation of A549 cells by enhancing the intracellular uptake of CUR. These results indicated that CUR-BCSC@PCs have great application prospects in cancer therapy as effective drug delivery carriers.

**Keywords:** Phycocyanin, Biotin, Chitosan oligosaccharide, Nanoparticles, A549 cells, Drug delivery

## Background

Chitosan oligosaccharide (COS) with the structure of β-(1-4)-linked *D*-glucosamines is a de-polymerization product prepared mainly by deacetylation and enzymatic hydrolysis of chitosan or chitin, which is derived from arthropod exoskeletons or the cell walls of fungi [1, 2]. It is worth noting that heavy metals and dyes can be removed by chitosan and its modified form of materials, in which chitosan acts as an adsorbent [3]. A number of studies have shown that COS possesses several biological properties, such as being anti-cancer, anti-inflammatory, anti-oxidative, and immunostimulatory [4]. COS is considered to be a non-toxic drug delivery carrier material, due to its biocompatibility, high water solubility, and chemical modifiability [5, 6].

In order to improve the solubility of hydrophobic anti-cancer drugs and reduce toxicity to normal tissues, medical researchers have been studying copolymers, which can self-assemble into micelles of a certain particle size range [7, 8]. These co-polymeric assemblies can reach and penetrate the tumor site passively or actively. Micelles are composed of two individual functional sections: the core, in which the hydrophobic drugs are encapsulated, and the outer shell or corona, which controls the in vivo pharmacokinetic properties [8]. Wang et al. [9] grafted deoxycholic acid onto COS chains through a chemical modification to form amphiphilic block copolymers, which could self-assemble into micelles in low-cost inorganic solvents. The hydrophobic core of the micelles contained quercetin, which greatly improved the water solubility of anti-cancer drugs and, in turn, enhanced quercetin's bioavailability.

Curcumin (CUR) is one of the main chemical constituents of turmeric [10]. In recent years, many researchers have studied the anti-cancer properties of CUR, and many studies have confirmed that this chemical can influence the growth of tumor cells via various signaling

* Correspondence: cdq1981@126.com
†Ziting Cheng and Wei Zhang contributed equally to this work.
[1]Collaborative Innovation Center of Advanced Drug Delivery System and Biotech Drugs, Universities of Shandong, Yantai University, Yantai, People's Republic of China
Full list of author information is available at the end of the article

pathways and enhance the immune system [11]. In addition, CUR is a photosensitizer with good photodynamic properties [12]. Thus, CUR is a promising drug for cancer therapy. However, its poor solubility, stability, and bioavailability limit its clinical application [13]. To mitigate these disadvantages, many researchers have improved the bioavailability of CUR through drug delivery systems. For example, Chen et al. [14] designed a new type of double pH-sensitive drug carrier, which enhanced the water solubility of CUR and improved its effect on tumor treatment.

Phycocyanin (PC), mainly obtained from cyanobacteria, is known as a water-soluble and light-harvesting pigment protein, which plays a role in capturing and transferring light into chemical energy during photosynthesis [15]. PC exerts multiple biological properties, such as being anticancerous [16], anti-inflammatory, and anti-oxidative that have attracted much attention in the fields of food and medicine [15, 17]. Hao et al. [16] discovered that PC inhibited non-small cell lung cancer cell growth by down-regulating toll/interleukin-1 receptor domain-containing adaptor protein (TIRAP). In addition, PC is also used in photodynamic therapy (PDT) of tumors as it is an excellent agent with no side effects [18–20]. The utilization of PC as fluorescent probes needs to be conjugated with specific identification elements such as biotin, antibodies, and streptavidin [21, 22]. Biotin, a water-soluble vitamin, is an essential micronutrient in the human body, which has tumor-targeting properties [23]. The biotin-specific receptor proteins, such as avidin, neutravidin, and streptavidin, are highly over-expressed on the surface of several cancer cells compared with that of normal cells [24, 25]. Thus, biotinylated nanoparticles have been extensively studied to be a drug delivery via receptor-mediated endocytosis [24].

In the present study, a novel type of PC functionalized nanocarrier was constructed, and the preparation of CUR-BCSC@PCs is presented in Fig. 1. The disulfide bond between COS and CUR contributed to the reductive sensitivity of the amphiphilic carrier material [26]. CUR was located in the hydrophobic inner core protected by the COS/PC shell. The interaction between biotin and PC and the electrostatic interaction, which was between positively charged COS and negatively charged PC, were used to modify PC onto the surface of CUR-BCSCs. CUR-BCSC@PCs were expected to reach tumor tissues due to improved permeability, the enhanced permeability and retention (EPR) effect, and the biotin receptor targeting effect [27]. In the tumor microenvironment, which has a higher glutathione concentration than normal cells, CUR-BCSC@PCs disintegrated through thiol–disulfide exchange reactions, achieving a high drug concentration in the tumor cells [23, 28, 29]. The CUR-BCSC@PC nano-delivery system described in this paper not only improved the bioavailability of CUR but also has the potential to be effective in the clinical treatment of tumors.

## Materials and Methods

### Materials

CUR was purchased from Zhanyun Chemical Co., Ltd. (Shanghai, China). COS was procured from Shandong Weikang Biomedical Science and Technology Co., Ltd.

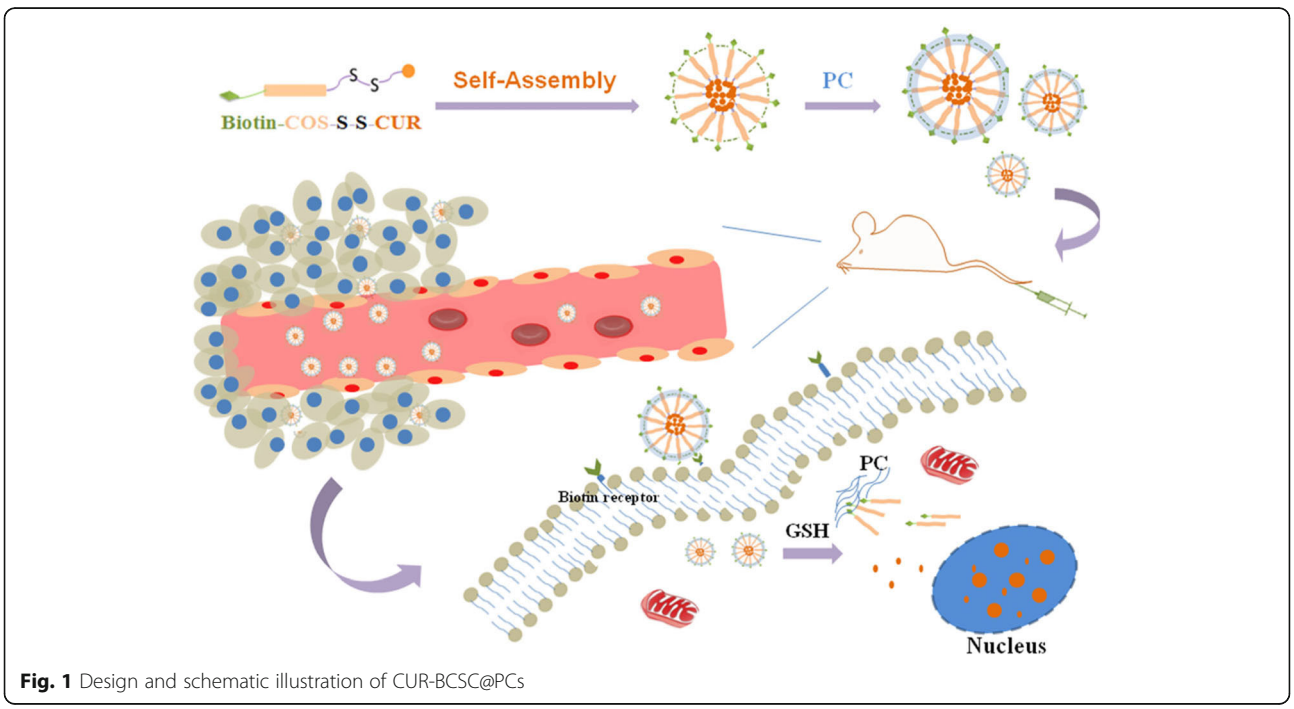


**Fig. 1** Design and schematic illustration of CUR-BCSC@PCs

PC was obtained from Zhejiang Binmei Biotechnology Co., Ltd. 3.3-Dithiodipropionic acid was obtained from Adamas Reagent Co., Ltd. (Shanghai, China). Carbonized carbodiimide hydrochloride (EDCI), dimethylamino pyridine (DMAP), tetrahydrofuran (THF), oxalyl chloride, and biotin were procured from Aladdin Chemistry Co., Ltd. L-Glutathione (GSH) and Hoechst 33342 were acquired from Sigma-Aldrich (Shanghai, China). Dialysis bags (MWCO 300 Da) were obtained from Beijing Biotopped Technology Co., Ltd. Formamide was prepared by Tianjin Fuyu Fine Chemical Co., Ltd. Deionized water was self-made in the laboratory.

An A549 cell line (human lung carcinoma cells) (Bena Culture Collection (Beijing, China)) was chosen to evaluate the cytotoxicity of the novel nanocarrier. A549 cells were grown in DMEM (Saiersi Biotechnology Co., Ltd. (Shangdong, Yantai, China)). Fetal bovine serum (FBS) was obtained from Hyclone (Logan, UT, USA). Penicillin and streptomycin were purchased from Sigma-Aldrich (Shanghai, China). 3-(4,5-dimethyl-2-thiazolyl)-2,5-diphenyl-2-H-tetrazolium bromide (MTT) was also procured from Sigma-Aldrich (Shanghai, China).

### Synthesis of CUR-BCSC@PCs

The synthetic routes used to prepare CUR-BCSC@PCs are shown in Fig. 2. The detailed experimental procedures are described below.

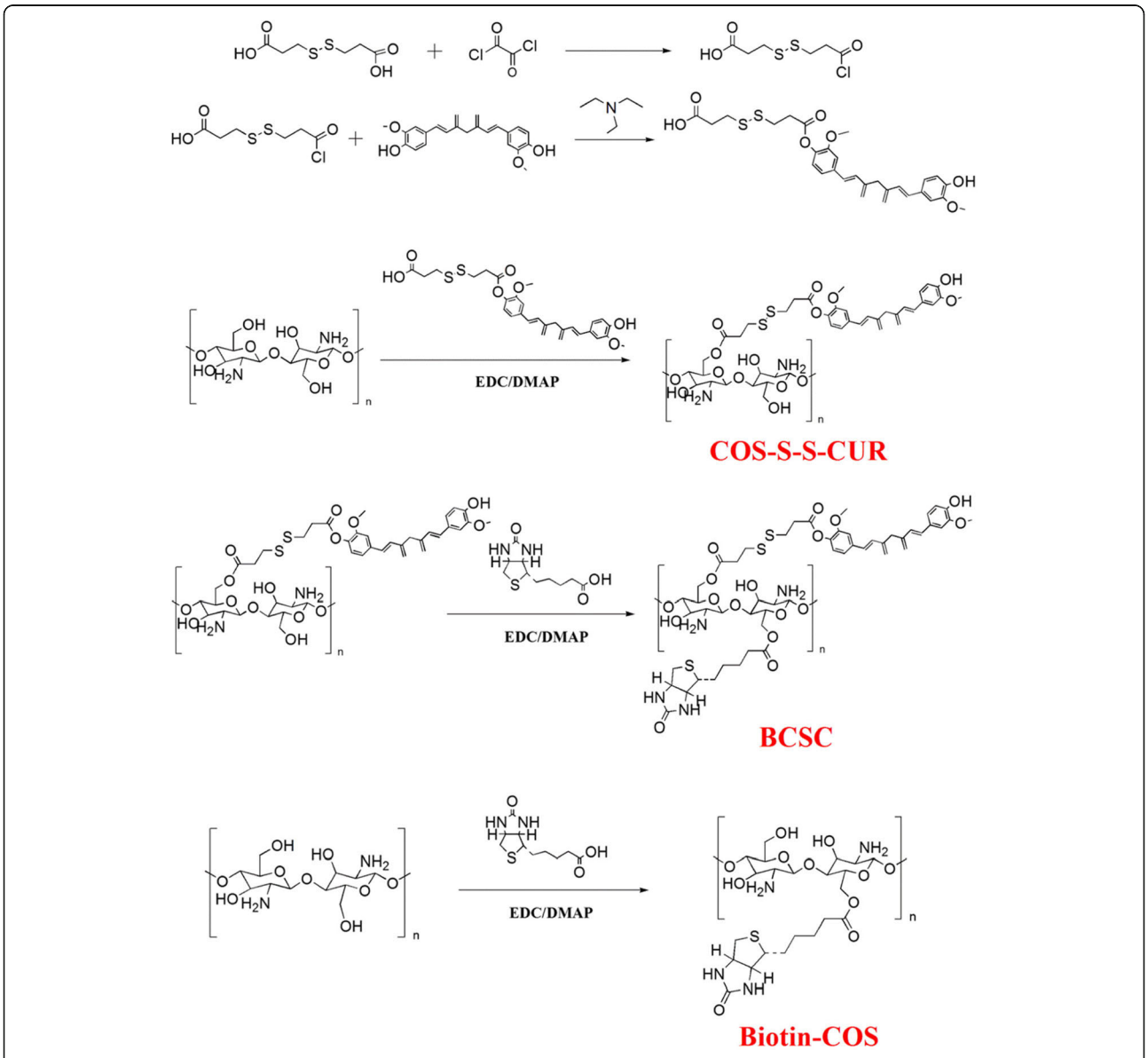


**Fig. 2** Synthetic route of COS-S-S-CUR, BCSC, and Biotin-COS

### Synthesis of COS-S-S-CUR

3.3-Dithiodipropionic acid-functionalized COS was synthesized by esterification catalyzed by acid chloride via a two-step reaction.

Step 1: 3.3-Dithiodipropionic acid (42.05 mg, 0.25 mmol) and dry THF (4 mL) were charged into a brown round-bottom flask, with a stirrer to dissolve the acid. Then, oxalyl chloride (0.3 mmol) diluted with THF was added to a flask, placed in an ice bath. The reaction was maintained at 35 °C. After stirring for 3 h, the unreacted oxalyl chloride was removed by rotary evaporation. Product 1 was prepared by the above steps. CUR was dissolved in 3 mL of THF, containing 34 μL of triethylamine, that was added dropwise to the flask containing product 1 under ice bath conditions and then stirred for 15 min. Subsequently, the mixture was stirred at 50 °C under a nitrogen atmosphere for 6 h. The obtained product was subjected to rotary distillation to remove triethylamine and THF and was then purified by column chromatography to acquire the pure product HOOC-S-S-CUR.

Step 2: The pure product HOOC-S-S-CUR was activated with EDCI (1.2 eq) and DMAP (1.2 eq) in formamide for 2 h. Subsequently, COS dissolved in 4 mL of formamide was added and stirred at 55 °C for 12 h. After the reaction was complete, the solution was dialyzed with a dialysis bag (MWCO 300 Da) and freeze-dried for 12 h.

### Synthesis of BCSC and Biotin-COS

In brief, biotin, EDCI, and DMAP were dissolved in 3 mL of formamide and transferred into a brown round-bottom flask. After stirring for 2 h at 30 °C, COS-S-S-CUR was dissolved in 3 mL of formamide and added dropwise into the flask. The reaction was maintained at 45 °C for 2 days. The final products were dialyzed (MWCO 300 Da) in deionized water and underwent centrifugation and lyophilization to obtain redox-sensitive BCSC. In addition, the synthesis of biotin-COS was conducted by the same method to link biotin to the COS chains.

$^{1}$H-NMR of COS-S-S-CUR, BCSC, and biotin-COS were measured using a mixture of DMSO-$D_6$ and $D_2O$ as the solvent.

### Preparation of CUR-Loaded BCSC Micelles (CUR-BCSCs)

CUR-BCSCs were prepared through the self-assembly method. Ten milligrams of BCSC was dissolved in 4 mL of formamide and then mixed with 1 mL of CUR solution (1 mg/mL) that was dissolved in formamide. The mixed solution was dialyzed using a dialysis bag (MWCO 300 Da) in deionized water for 24 h and the deionized water was changed every 2 h. CUR-BCSCs were filtrated using millipore membranes of 800 nm, 450 nm, and 220 nm.

### Preparation of CUR-BCSC@PCs

The prepared CUR-BCSCs were mixed with an aqueous solution of PC (1.0 mg/mL) and incubated for 30 min at 4 °C. Subsequently, PC was removed using a 100 kDa centrifugal filter and rinsed with water three times. The final product (CUR-BCSC@PC) was stored at 4 °C in darkness for further study.

### Characterizations

Dynamic laser scattering (DLS) measurements were carried out on a Particle Analyzer Delsa Nano C (Beckman Coulter Inc.) to observe the particle size, zeta potential, and polydispersity index (PI). The morphology of CUR-BCSCs and CUR-BCSC@PCs was confirmed by transmission electron microscopy (TEM, H-600; Hitachi, Tokyo, Japan) measurements.

### Encapsulation Efficiency (EE) and Drug Loading Capacity (DL)

HPLC (Agilent 1260GB12C) was used to determine the EE and DL of nanoparticles. First, 2 mL of CUR-BCSCs or CUR-BCSC@PCs was mixed with 3 mL of acetonitrile and demulsified by ultrasound, in which acetonitrile was then added to 10 mL. Before the measurement, the column temperature of the Phenomenex C18 column (250 mm × 4.6 mm, 5 um) was adjusted to 25 °C, while the flow rate of the mobile phase was set to 1.0 mL·min$^{-1}$. The ratio of 0.5% glacial acetic acid to acetonitrile was 40:60 (v/v). In the detection process, with a detection wavelength of 425 nm, 20 μL of samples was injected [30]. The following formula was used to calculate the EE and DL:

$$\mathrm{EE}\% = (\text{Weight of Cur in the nanoparticles}/\text{Weight of the feeding Cur}) \times 100\%$$

$$\mathrm{DL}\% = (\text{Mass of Cur in the nanoparticles}/\text{Mass of the nanoparticles}) \times 100\%$$

### In vitro Stability Test

Phosphate-buffered saline (PBS) containing GSH (0, 20 μM, 10 mM) was prepared and treated with CUR-BCSC@PCs for 4 h to observe the changes in particle size under different concentrations of glutathione at 37 °C. In addition, the hydrodynamic diameter of CUR-BCSC@PCs was investigated in PBS solution using a Particle Analyzer Delsa Nano C (Beckman Coulter Inc.) at 37 °C at different time points (4, 8, 12, and 24 h).

### In vitro CUR Release from CUR-BCSC@PCs

The in vitro CUR release behaviors of CUR-BCSC@PCs were investigated using the dialysis method. PBS solutions containing glutathione (GSH: 20 μmol/L, 1 mmol/L, 5 mmol/L, 10 mmol/L) were prepared, and 0.5% Tween 80 was added. PBS buffer (45 mL), containing different concentrations of GSH, was added to 50 mL centrifuge tubes;

then, a dialysis bag containing 1 mL of CUR-BCSC@PCs was placed in each centrifuge tube, which was shaken at 37 °C. At different time points (0.2, 1, 4, 8, 12, 24, 48, 72 h), 2 mL of release medium was collected, and fresh release medium of the same type was added to keep its volume unchanged. HPLC was used to determine the concentration of CUR in the collected release medium.

### Cell Culture

The human lung carcinoma A549 cells were cultured in DMEM, which included 10% FBS and 1% penicillin-streptomycin, and were incubated at 37 °C in 5% $CO_2$ atmosphere [31, 32].

### In vitro Cellular Proliferation Inhibition

The in vitro cytotoxicity of CUR, BCSC micelles (BCSCs), CUR-BCSCs, and CUR-BCSC@PCs against the A549 cell line was evaluated using a standard MTT assay [33]. The A549 cells were seeded in 96-well plates (5000 cells per well) for 24 h to adhere to the wall. The original medium was discarded, and then 100 μL of fresh medium containing free CUR, BCSCs, CUR-BCSCs, and CUR-BCSC@PCs (0.1, 1, 5, 10, 15, and 20 μg/mL based on CUR) was added and cultured for 24 h. Wells without administration were used as blank controls. The cells were subjected to MTT assay by removing the medium and adding 20 μL of MTT solution (5 mg/mL). After incubation for another 4 h at 37 °C in 5% $CO_2$ atmosphere, the MTT solution was replaced with 150 μL of DMSO to dissolve the purple MTT-formazan. Subsequently, a microplate reader (Thermo Fisher Scientific Co., Waltham, MA) was used to measure the absorbance of each well at 570 nm.

### In vitro Cell Uptake and Localization

The cellular uptake ability of CUR-BCSCs and CUR-BCSC@PCs was investigated under a fluorescence microscope (FM, Eclipse E400; Nikon Corporation, Tokyo, Japan). A549 cells were seeded in 24-well plates at $4 \times 10^4$ cells per well and were co-incubated with CUR-BCSCs and CUR-BCSC@PCs (CUR concentration: 20 μg/mL) at 37 °C in a humidified atmosphere containing 5% $CO_2$ for 1, 2, and 4 h. The A549 cells were washed with PBS three times after removing the culture

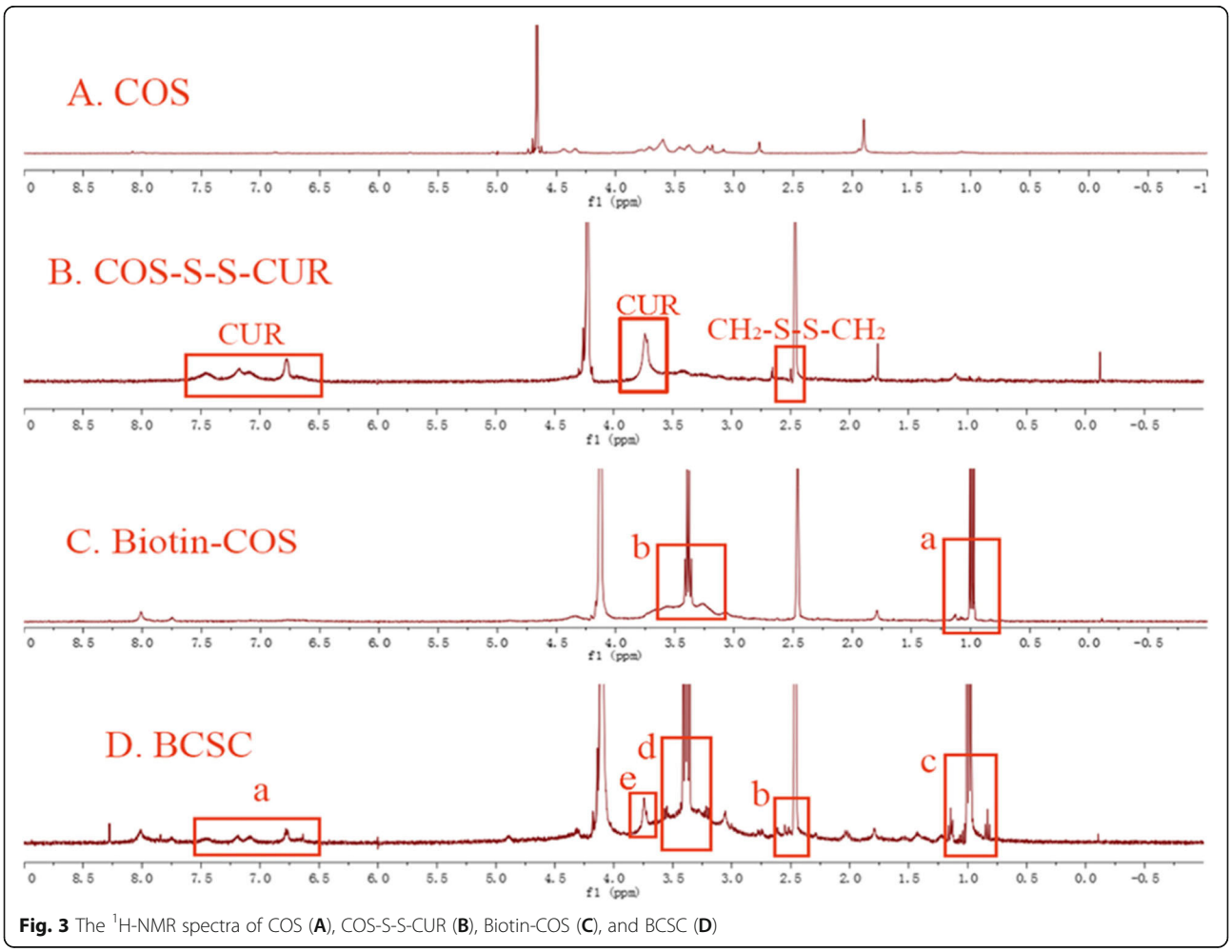


**Fig. 3** The $^1$H-NMR spectra of COS (**A**), COS-S-S-CUR (**B**), Biotin-COS (**C**), and BCSC (**D**)

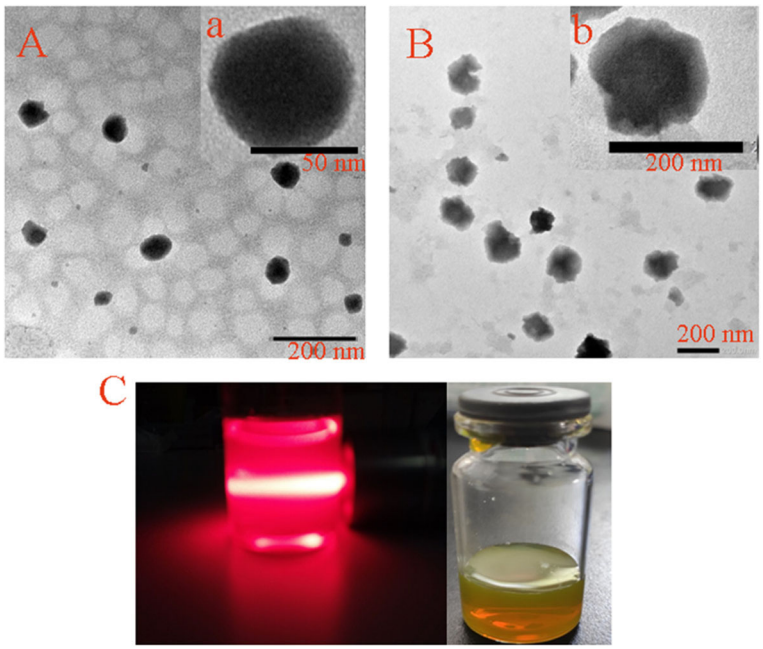


**Fig. 4** **A** The TEM images of CUR-BCSCs and a single CUR-BCSC. **B** The TEM images of CUR-BCSC@PCs and a single CUR-BCSC@PC. **C** Tyndall effect and the photograph of CUR-BCSC@PCs in water

media containing drugs. Then, PBS containing 4% paraformaldehyde was added for 20 min and washed with PBS for another three times. The cell nuclei were stained by Hoechst 33342 for 15 min and observed using an inverted fluorescence microscope.

### Statistical Analysis

All experiments were carried out at least three times and expressed as means ± SD. Statistical tests were analyzed using the Student's $t$ test. $P < 0.05$ was set as statistically significant, and $P < 0.01$ was considered highly significant.

## Results and Discussion

### Characterization of COS, COS-S-S-CUR, Biotin-COS, and BCSC

The main characteristic resonances of CUR and $CH_2$-S-S-$CH_2$ appeared on the $^1$H-NMR spectrum of COS-S-S-CUR, proving the successful conjugation of CUR to the COS chains. Compared with the peaks of COS in Fig. 3(A), the characteristic signals of CUR presented in Fig. 3(B) were observed in the region between 6.7 and 7.5 ppm and at 3.75 ppm (–$OCH_3$), while the resonance of $CH_2$-S-S-$CH_2$ at 2.5 ppm was unchanged. As shown in (Fig. 3(C), a, b), the peaks of biotin on the $^1$H-NMR spectrum of Biotin-COS were 0.99 ppm (–$CH_2$–) and 3.39 ppm (–CH–S–). $^1$H-NMR spectrum of BCSC is shown in Fig. 3(D). The resonances of CUR (Fig. 3(D), a, e) were seen in the corresponding positions, and the characteristic peak of $CH_2$-S-S-$CH_2$ (Fig. 3(D), b) was again observed at 2.5 ppm. In addition, the appearance of signals at peak 0.09 ppm and 3.39 ppm (Fig. 3(D), c, d) verified the existence of biotin linked to the COS-S-S-CUR chains. The characteristic resonances of CUR, $CH_2$-S-S-$CH_2$, and biotin as shown in Fig. 3(D) are consistent with those in Fig. 3(B) and Fig. 3(C), indicating that the amphiphilic material BCSC was synthesized successfully.

### Characterization of CUR-BCSCs and CUR-BCSC@PCs

The morphologies of CUR-BCSCs and CUR-BCSC@PCs were studied by transmission electron microscopy (TEM) (Fig. 4(A, B)). CUR-BCSCs showed a smooth spherical shape (Fig. 4(A), a) under electron microscopy, while CUR-BCSC@PCs possessed an approximately spherical shape with the blooming layer surrounding the CUR-BCSC@PCs (Fig. 4(B), b). This indicated that PC formed a protein corona structure by covering the surfaces of CUR-BCSCs. A clear Tyndall effect of CUR-

**Table 1** The physiochemical properties of CUR-BCSCs and CUR-BCSC@PCs ($n = 3$)

| Preparation | Size (nm) | PI | Zeta (mV) | DL (%) | EE (%) |
|---|---|---|---|---|---|
| CUR-BCSCs | 97.8 ± 4.2 | 0.181 ± 0.014 | 21.57 ± 0.53 | 7.8 ± 1.08 | 48.84 ± 7.41 |
| CUR-BCSC@PCs | 160.3 ± 9.0 | 0.114 ± 0.024 | 12.90 ± 1.93 | 5.3 ± 0.67 | 52.24 ± 5.50 |

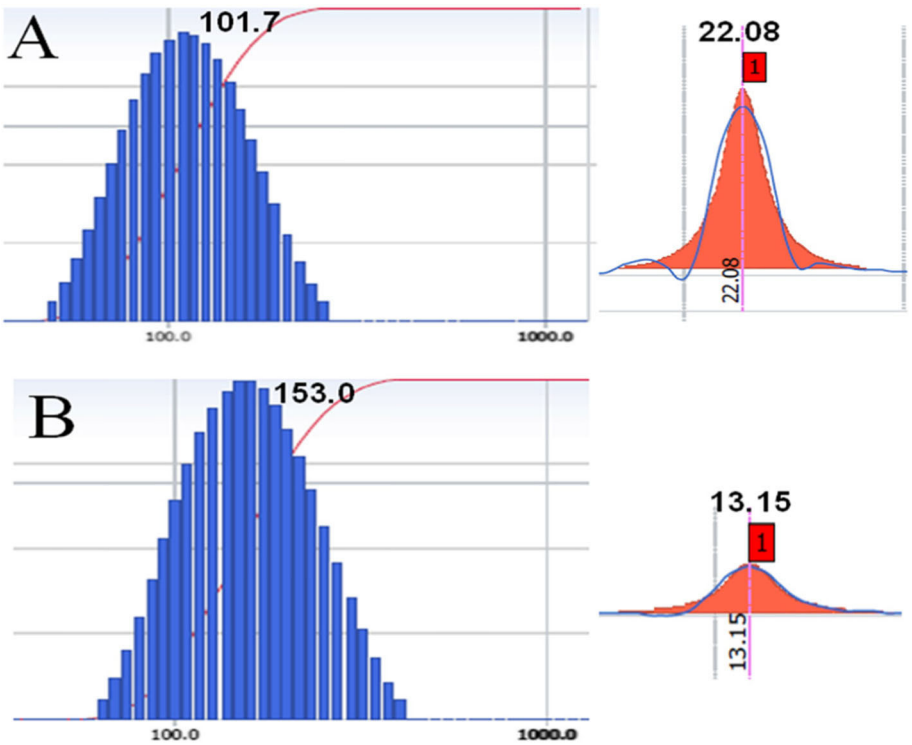


**Fig. 5** **a** The size distribution and the zeta potential of CUR-BCSCs; **b** The size distribution and the zeta potential of CUR-BCSC@PCs

BCSC@PCs was observed because of the existence of generous nanoparticles (Fig. 4(C)). The particle size, PI, zeta potential, DL (%), and EE (%) of CUR-BCSCs and CUR-BCSC@PCs are illustrated in Table 1. In Fig. 5, the average size of CUR-BCSCs and CUR-BCSC@PCs was 97.8 ± 4.2 nm and 160.3 ± 9.0 nm, respectively. Meanwhile, the PI values of CUR-BCSCs and CUR-BCSC@PCs were 0.181 ± 0.014 and 0.114 ± 0.024, respectively, which are smaller than 0.2, indicating the uniformity of their sizes. The zeta potentials of CUR-BCSCs and CUR-BCSC@PCs were 21.57 ± 0.53 and 12.90 ± 1.93 mV, respectively. Due to the electronegative PC coating, the zeta potential of CUR-BCSCs was higher than that of CUR-BCSC@PCs. The EE of CUR-BCSC@PCs was higher than that of CUR-BCSCs.

### Stability of CUR-BCSC@PCs

As shown in Fig. 6a, due to the reductive nature of the disulfide bond, the bond was cleaved in PBS containing 10 mM GSH, and CUR-BCSC@PCs were disintegrated into polymer fragments, which agglomerated to increase the

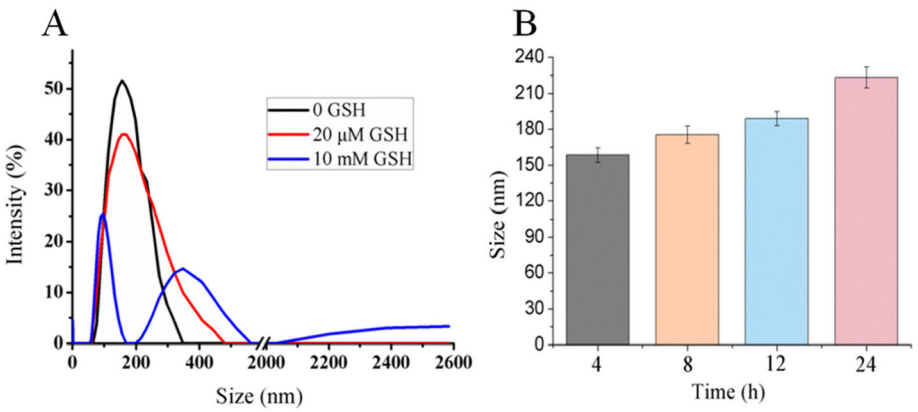


**Fig. 6** The stability of CUR-BCSC@PCs. **a** Size changes of CUR-BCSC@PCs at different GSH concentration. **b** Size changes of CUR-BCSC@PCs in PBS at different times

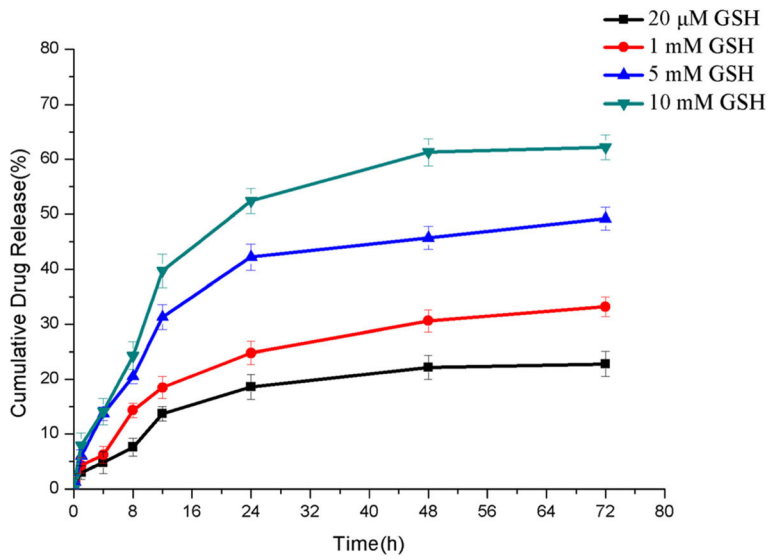


**Fig. 7** Cumulative release of CUR from CUR-BCSC@PCs at different GSH conditions

particle size of the nanoparticles. However, in PBS containing 20 μM GSH, the changes in particle size were minor, which showed a similar result to PBS without GSH. As illustrated in Fig. 6b, particle size was measured at different times to study the stability of CUR-BCSC@PCs in PBS, and the results showed that the particle size of CUR-BCSC@PCs increased slowly over time [14].

### Reduction Response of CUR-BCSC@PCs

It is well established that disulfide bonds are unstable in a tumor-reductive environment. Researchers have used disulfide bonds to connect hydrophilic polymers and hydrophobic drugs to prepare amphiphilic fragments, which can self-assemble in water to form nano-micelles. Then, according to differences in the physiological environment and the tumor environment, disulfide bonds break up at the tumor site to release drugs [34]. In the present study, in vitro drug release was conducted to verify whether CUR-BCSC@PCs could present an expected release property. The reduction response ability of CUR-BCSC@PCs containing disulfide linkages was investigated following the activation of GSH. As shown in Fig. 7, the release of CUR from CUR-BCSC@PCs in the medium with 20 μM GSH at pH 7.4, which simulated

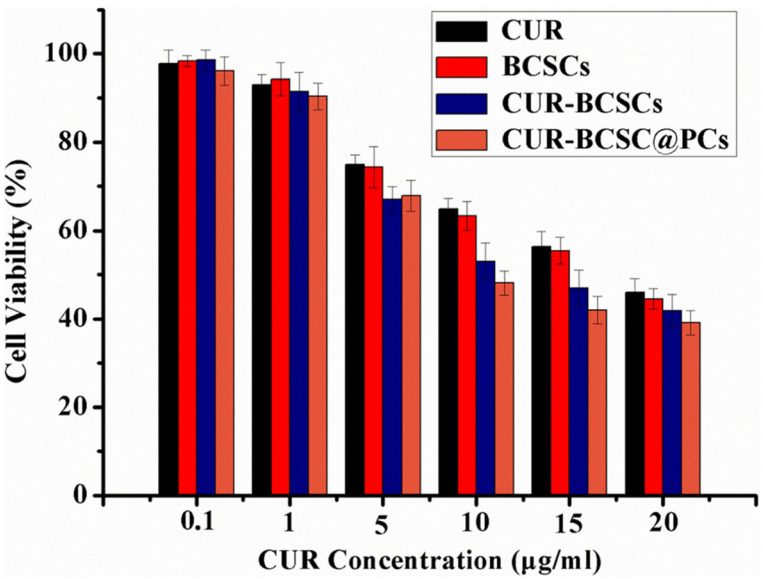


**Fig. 8** In vitro cytotoxicity of different formulations at 24 h in A549 cells

the extracellular environment, was extremely slow compared with an environment with 10 mM GSH at pH 7.4. Furthermore, compared with the 20 μM GSH medium, the 1, 5, and 10 mM GSH showed significant differences in release behavior. With the increase in GSH concentration, the release of CUR from CUR-BCSC@PCs was also promoted, indicating that the drug release was in response to the GSH concentration.

### In vitro Cytotoxicity

MTT assay was conducted to investigate the cytotoxic effects of free CUR, BCSCs, CUR-BCSCs, and CUR-BCSC@PCs on A549 cell lines [35]. The cell viability data is summarized in Fig. 8. All the CUR preparations showed dose dependence in terms of cell proliferation inhibition. As shown in Fig. 8, free CUR had slightly less capability for inhibiting cellular proliferation against all A549 cells compared with CUR-BCSC@PCs and CUR-BCSCs, after incubation for 24 h. For A549 cells, the anti-cancer activity of CUR-BCSC@PCs was better than that of BCSCs and CUR-BCSCs, which was likely due to excellent cell uptake. Furthermore, CUR-BCSC@PCs showed a higher cytotoxicity property than CUR-BCSCs, indicating that PC has a potential inhibitory effect on the proliferation of A549 cells.

### In vitro Cell Uptake Study

As shown in Fig. 8, the fluorescence signals of CUR were observed in A549 cells treated with CUR-BCSCs and CUR-BCSC@PCs (CUR: 20 μg/mL) at 1, 2, and 4 h, using the inverted fluorescence microscope. CUR, as a green fluorescence probe, was also an anti-cancer drug, which was frequently used as a hydrophobic model drug to develop new and efficient drug delivery systems. As illustrated in Fig. 9a, both CUR-BCSCs and CUR-BCSC@PCs were absorbed in A549 cell lines, and the uptake efficiency was time-dependent. Owing to the over-expressed biotin receptors on the surface of cancer cells, biotin-loaded nano-micelles had an affinity for A549 cells. The fluorescence signals from CUR-BCSC@PCs were high at 4 h,

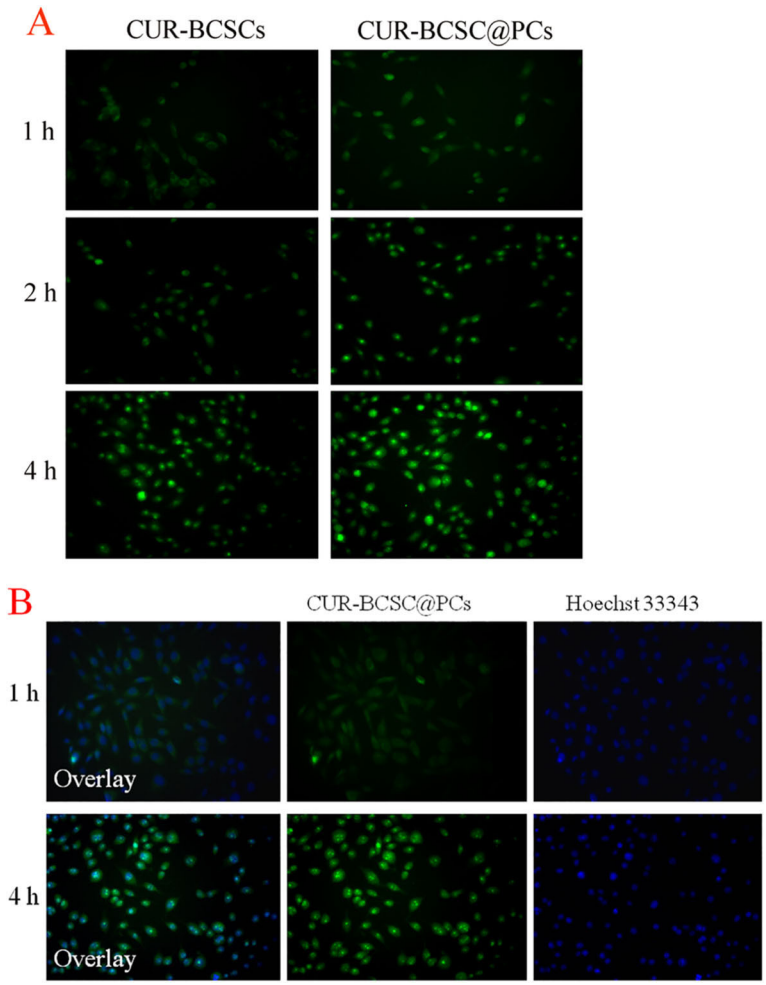


**Fig. 9** **a** Fluorescent imaging of the cellular uptake of CUR-BCSCs and CUR-BCSC@PCs at different times. **b** The cell location of CUR-BCSC@PCs at 1 h and 4 h

indicating a high cell uptake rate of CUR-BCSC@PCs. The fluorescence signals of CUR-BCSC@PCs were higher at 4 h than that at 1 h or 2 h; this proved that the cell uptake was time-dependent.

The nuclei of A549 cells were stained by Hoechst 33342. As shown in Fig. 9b, green fluorescence signals were seen in the cytoplasm of the 1 h group of CUR-BCSC@PCs, and the fluorescence gradually occurred in the nuclei of the 4 h group of CUR-BCSC@PCs, which demonstrated cellular uptake through caveolae-mediated endocytosis.

## Conclusions

In this study, a type of protein-functionalized COS nanoparticle was prepared through condensation reactions, self-assembling behavior, and the interaction between PC and CUR-BCSCs. After the preliminary investigation, the amphiphilic carrier materials (BCSCs) with redox sensitivity were synthesized successfully and verified using $^{1}$H-NMR. The surfaces of CUR-BCSCs were modified with a layer of phycocyanin corona, which could improve the cell uptake efficiency and protect CUR-BCSC@PCs from plasma protein adsorption. The cellular cytotoxicity and uptake analysis indicated that CUR-BCSC@PCs could transport CUR into the A549 cells and has an excellent anti-proliferative property. Considering the PDT effect of PC and CUR, we will evaluate photodynamic properties and anti-cancer activity of CUR-BCSC@PCs under phototherapy in the next phase of this research. This study paved the way for the improvement of anti-cancer drug efficacy and the introduction of a functional protein corona. In summary, the nanomedicine carrier biomaterial of CUR-BCSC@PCs based on COS with multiple functions has provided a new strategy for tumor treatment and exhibited great application prospects.

### Abbreviations

BCSC: Biotin-chitosan oligosaccharide-dithiodipropionic acid-curcumin; COS: Chitosan oligosaccharide; COS-S-S-CUR: Chitosan oligosaccharide-dithiodipropionic acid-curcumin; CUR: Curcumin; CUR-BCSC@PCs: Phycocyanin-functionalized and curcumin-loaded biotin-chitosan oligosaccharide-dithiodipropionic acid-curcumin micelles; CUR-BCSCs: Curcumin-loaded biotin-chitosan oligosaccharide-dithiodipropionic acid-curcumin micelles; EPR: Enhanced permeability and retention; PC: Phycocyanin; PDT: Photodynamic therapy

### Acknowledgements

We would like to acknowledge and thank Dr. Zongliang Liu for providing access and analysis to $^{1}$H-NMR for our studies. In addition, we would like to thank Editage (www.editage.cn) for English language editing.

### Authors' Contributions

ZTC, WZ, YPZ, PZ, and DQC conceived of the study and participated in its design of Phycocyanin-functionalized Chitosan Oligosaccharide Nanoparticles for anticancer treatment, Their Stability and Cellular Behavior. XYH, BJW, and FZ participated in the cytotoxicity assays and cell uptake test. All authors read and approved the final manuscript.

### Funding

This work was supported by Taishan Scholar Program (No. qnts20161035) and Shandong Provincial Natural Science Foundation for Outstanding Young Scholar (No. ZR2019YQ30).

### Availability of Data and Materials

The conclusions made in this manuscript are based on the data which are all presented and shown in this paper.

### Competing Interests

The authors declare that they have no competing interests.

### Author details

[1]Collaborative Innovation Center of Advanced Drug Delivery System and Biotech Drugs, Universities of Shandong, Yantai University, Yantai, People's Republic of China. [2]Department of Radiotherapy, Affiliated Yantai Yuhuangding Hospital of Qingdao University, Yantai, Shandong, People's Republic of China.

Received: 6 September 2019 Accepted: 12 November 2019
Published online: 21 December 2019

### References

1. Muanprasat C, Chatsudthipong V (2017) Chitosan oligosaccharide: biological activities and potential therapeutic applications. Pharmacol Ther 170:80–97
2. Yuan XB, Zheng JP, Jiao SM, Cheng G, Feng C, Du YG, Liu HT (2019) A review on the preparation of chitosan oligosaccharides and application to human health, animal husbandry and agricultural production. Carbohydr Polym 220:60–70
3. Samuel MS, Shah SS, Subramaniyan V, Qureshi T, Bhattacharya J, Pradeep Singh ND (2018) Preparation of graphene oxide/chitosan/ferrite nanocomposite for chromium (VI) removal from aqueous solution. Int J Biol Macromol 119:540–547
4. Naveed M, Phil L, Sohail M, Hasnat M, Baig MMFA, Ihsan AU, Shumzaid M, Kakar MU, Mehmood Khan T, Akabar MD, Hussain MI, Zhou Q-G (2019) Chitosan oligosaccharide (COS): an overview. Int J Biol Macromol 129:827–843
5. Manivasagan P, Bharathiraja S, Santha Moorthy M, Mondal S, Nguyen TP, Kim H, Phan TTV, Lee KD, Oh J (2018) Biocompatible chitosan oligosaccharide modified gold nanorods as highly effective photothermal agents for ablation of breast cancer cells. Polymers 10:232
6. De Oliveira PR, Goycoolea FM, Pereira S, Schmitt CC, Neumann MG (2018) Synergistic effect of quercetin and pH-responsive DEAE-chitosan carriers as drug delivery system for breast cancer treatment. Int J Biol Macromol 106:579–586
7. Cabral H, Kataoka K (2014) Progress of drug-loaded polymeric micelles into clinical studies. J Control Release 190:465–476
8. Gothwal A, Khan I, Gupta U (2016) Polymeric micelles: recent advancements in the delivery of anticancer drugs. Pharm Res 33:18–39
9. Wang H, Yang ZM, He ZY, Zhou C, Wang C, Chen Y, Liu XW, Li SD, Li PW (2019) Self-assembled amphiphilic chitosan nanomicelles to enhance the solubility of quercetin for efficient delivery. Colloids Surf B Biointerfaces 179:519–526
10. Zhao SJ, Pi C, Ye Y, Zhao L, Wei YM (2019) Recent advances of analogues of curcumin for treatment of cancer. Eur J Med Chem 180:524–535
11. Shafabakhsh R, Pourhanifeh MH, Mirzaei HR, Sahebkar A, Asemi Z, Mirzaei H (2019) Targeting regulatory T cells by curcumin: a potential for cancer immunotherapy. Pharmacol Res 147:104353
12. Sun MD, Zhang Y, He Y, Xiong MH, Huang HY, Pei SC, Liao JF, Wang YS, Shao D (2019) Green synthesis of carrier-free curcumin nanodrugs for light-activated breast cancer photodynamic therapy. Colloids Surf B Biointerfaces 180:313–318
13. Peng SF, Li ZL, Zou LQ, Liu W, Liu CM, McClements DJ (2018) Enhancement of curcumin bioavailability by encapsulation in sophorolipid-coated nanoparticles: an in vitro and in vivo study. J Agric Food Chem 66:1488–1497
14. Chen DQ, Song XY, Wang KL, Guo CJ, Yu YM, Fan HY, Zhao F (2017) Design and evaluation of dual CD44 receptor and folate receptor-targeting double-smart pH-response multifunctional nanocarrier. J Nanopart Res 19:400
15. Yu P, Wu YT, Wang GW, Jia TM, Zhang YS (2017) Purification and bioactivities of phycocyanin. Crit Rev Food Sci Nutr 57:3840–3849
16. Hao S, Li S, Wang J, Yan Y, Ai X, Zhang JW, Ren YQ, Wu TT, Liu LY, Wang CT (2019) Phycocyanin exerts anti-proliferative effects through down-regulating

TIRAP/NF-kappaB activity in human non-small cell lung cancer cells. Cells 8: 588
17. Jiang LQ, Wang YJ, Zhu F, Liu GX, Liu HH, Ji HH, Zheng SH, Li B (2019) Molecular mechanism of anti-cancer activity of the nano-drug C-PC/CMC-CD59sp NPs in cervical cancer. J Cancer 10:92–104
18. Bharathiraja S, Manivasagan P, Santha Moorthy M, Bui NQ, Jang B, Phan TTV, Jung W-K, Kim Y-M, Lee KD, Oh J (2018) Photo-based PDT/PTT dual model killing and imaging of cancer cells using phycocyanin-polypyrrole nanoparticles. Eur J Pharm Biopharm 123:20–30
19. Lin ZX, Jiang B-P, Liang JZ, Wen CC, Shen X-C (2019) Phycocyanin functionalized single-walled carbon nanohorns hybrid for near-infrared light-mediated cancer phototheranostics. Carbon 143:814–827
20. Agrawal M, Yadav SK, Agrawal SK, Karmakar S (2017) Nutraceutical phycocyanin nanoformulation for efficient drug delivery of paclitaxel in human glioblastoma U87MG cell line. J Nanopart Res 19:272
21. Cai YA, Murphy JT, Wedemayer GJ, Glazer AN (2001) Recombinant phycobiliproteins. Anal Biochem 290:186–204
22. Wu J, Chen HX, Jiang P (2018) Chromophore attachment to fusion protein of streptavidin and recombinant allophycocyanin alpha subunit. Bioengineered 9:108–115
23. Lu RX, Zhou L, Yue QM, Liu QJ, Cai XJ, Xiao WJ, Hai L, Guo L, Wu Y (2019) Liposomes modified with double-branched biotin: a novel and effective way to promote breast cancer targeting. Bioorg Med Chem 27:3115–3127
24. Vinothini K, Rajendran NK, Munusamy MA, Alarfaj AA, Rajan M (2019) Development of biotin molecule targeted cancer cell drug delivery of doxorubicin loaded kappa-carrageenan grafted graphene oxide nanocarrier. Mater Sci Eng C Mater Biol Appl 100:676–687
25. Gebremedhin KH, Li ML, Gao FL, Gurram B, Fan JL, Wang JY, Li YM, Peng XJ (2019) Benzo [a]phenoselenazine-based NIR photosensitizer for tumor-targeting photodynamic therapy via lysosomal-disruption pathway. Dyes Pigments 170:107617
26. Shi CL, Guo X, Qu QQ, Tang ZM, Wang Y, Zhou SB (2014) Actively targeted delivery of anticancer drug to tumor cells by redox-responsive star-shaped micelles. Biomaterials 35:8711–8722
27. Jin HJ, Jin Q, Liang ZH, Liu YQ, Qu XJ, Sun QJ (2019) Quantum dot based fluorescent traffic light nanoprobe for specific imaging of avidin-type biotin receptor and differentiation of cancer cells. Anal Chem 91:8958–8965
28. Lv SX, Tang ZH, Zhang DW, Song WT, Li MQ, Lin J, Liu HY, Chen XS (2014) Well-defined polymer-drug conjugate engineered with redox and pH-sensitive release mechanism for efficient delivery of paclitaxel. J Control Release 194:220–227
29. Chuan XX, Song Q, Lin JL, Chen XH, Zhang H, Dai WB, He B, Wang XQ, Zhang Q (2014) Novel free-paclitaxel-loaded redox-responsive nanoparticles based on a disulfide-linked poly (ethylene glycol)-drug conjugate for intracellular drug delivery: synthesis, characterization, and antitumor activity in vitro and in vivo. Mol Pharm 11:3656–3670
30. Dong X, Zou SH, Guo CJ, Wang KL, Zhao F, Fan HY, Yin JG, Chen DQ (2018) Multifunctional redox-responsive and CD44 receptor targeting polymer-drug nanomedicine based curcumin and alendronate: synthesis, characterization and in vitro evaluation. Artif Cells Nanomed Biotechnol 46:168–177
31. Karolina U, Malgorzata A, Magdalena J, Malgorzata J, Rafal R, Xuecheng C, Ewa M (2014) Chemical and magnetic functionalization of graphene oxide as a route to enhance its biocompatibility. Nanoscale Res Lett 9:656
32. Chang YL, Yang ST, Liu JH, Dong E, Wang YW, Cao A, Liu YF, Wang HF (2011) In vitro toxicity evaluation of graphene oxide on A549 cells. Toxicol Lett 200:201–210
33. Parthiban C, Pavithra M, Reddy LVK, Sen D, Samuel SM, Singh NDP (2018) Visible-light-triggered fluorescent organic nanoparticles for chemo-photodynamic therapy with real-time cellular imaging. ACS Appl Nano Mater 1:6281–6288
34. Yu YM, Zou SH, Wang KL, Liang RC, Fan XX, Wang BJ, Liu MN, Fang L, Liu WH, Wu ZM, Chen DQ (2018) Synthesis, characterization and in vitro evaluation of dual pH/redox sensitive marine laminarin-based nanomedicine carrier biomaterial for cancer therapy. J Biomed Nanotechnol 14:1568–1577
35. Samuel MS, Shah SS, Bhattacharya J, Subramaniam K, Pradeep Singh ND (2018) Adsorption of Pb (II) from aqueous solution using a magnetic chitosan/graphene oxide composite and its toxicity studies. Int J Biol Macromol 115:1142–1150

## Publisher's Note